Journal of Geophysical Research: Atmospheres

RESEARCH ARTICLE
10.1029/2018JD028293

Inferring Surface Albedo Prediction Error Linked to Forest Structure at High Latitudes

Ryan M. Bright[1], Stephanie Eisner[1,2], Marianne T. Lund[3], Titta Majasalmi[1], Gunnar Myhre[3], and Rasmus Astrup[1]

[1]Norwegian Institute of Bioeconomy Research (NIBIO), Ås, Norway, [2]Norwegian Water and Energy Directorate (NVE), Oslo, Norway, [3]Centre for International Climate and Environmental Research – Oslo (CICERO), Oslo, Norway

Key Points:
- Absolute surface albedo prediction error due to insufficient characterization of forest structure can be as large as 0.19 in Fennoscandia
- Winter (December–March) radiative forcing of albedo prediction error linked to forest structure is 0.4 W/m^2 for a spatial domain of 611,000 km^2
- Neglecting forest albedo transitions when simulating forest management can lead to large shortwave energy balance prediction error

Correspondence to:
R. M. Bright,
ryan.bright@nibio.no

Citation:
Bright, R. M., Eisner, S., Lund, M. T., Majasalmi, T., Myhre, G., & Astrup, R. (2018). Inferring surface albedo prediction error linked to forest structure at high latitudes. *Journal of Geophysical Research: Atmospheres*, *123*, 4910–4925. https://doi.org/10.1029/2018JD028293

Received 8 JAN 2018
Accepted 21 APR 2018
Accepted article online 30 APR 2018
Published online 17 MAY 2018

Abstract Predicting the surface albedo of a forest of a given species composition or plant functional type is complicated by the wide range of structural attributes it may display. Accurate characterizations of forest structure are therefore essential to reducing the uncertainty of albedo predictions in forests, particularly in the presence of snow. At present, forest albedo parameterizations remain a nonnegligible source of uncertainty in climate models, and the magnitude attributable to insufficient characterization of forest structure remains unclear. Here we employ a forest classification scheme based on the assimilation of Fennoscandic (i.e., Norway, Sweden, and Finland) national forest inventory data to quantify the magnitude of the albedo prediction error attributable to poor characterizations of forest structure. For a spatial domain spanning ~611,000 km^2 of boreal forest, we find a mean absolute wintertime (December–March) albedo prediction error of 0.02, corresponding to a mean absolute radiative forcing ~0.4 W/m^2. Further, we evaluate the implication of excluding albedo trajectories linked to structural transitions in forests during transient simulations of anthropogenic land use/land cover change. We find that, for an intensively managed forestry region in southeastern Norway, neglecting structural transitions over the next quarter century results in a foregone (undetected) radiatively equivalent impact of ~178 Mt-CO_2-eq. year^{-1} on average during this period—a magnitude that is roughly comparable to the annual greenhouse gas emissions of a country such as The Netherlands. Our results affirm the importance of improving the characterization of forest structure when simulating surface albedo and associated climate effects.

Plain Language Summary Surface albedo—or the ratio of reflected to incoming sunlight—is an important physical property of the climate system and, as such, requires skillful prediction by climate models. Predicting the surface albedo in a forest during months with snow is complicated by many factors, among which is the sufficiency by which a forest's physical properties are represented in the model. This study makes use of detailed national forest inventory information to estimate the contribution to albedo prediction error that may be wholly attributed to insufficient characterizations of forest structure in a climate model, which we find to be nonnegligible. This study also investigates the consequence of ignoring structural transitions in forests when predicting future surface albedo impacts of forest management activities in climate modeling studies. For a case study region in southeast Norway, we find that not accounting for differences in surface albedo between forests in various development states can result in substantial climate effects going undetected, with magnitudes on the order of the annual greenhouse gas emissions of some European countries such as The Netherlands, or approximately 2 days of current global CO_2 emissions.

1. Introduction

Amplification of CO_2-forced warming at high latitudes is strongly linked to the surface albedo feedback or the extra absorption of shortwave (SW) radiation as melting snow and ice expose darker surfaces (Budyko, 1969; Hall, 2004; W. D. Sellers, 1969; Winton, 2006). Our confidence to predict global climate change connected to anthropogenic greenhouse gas emissions is therefore directly tied to the skillfulness by which climate models predict (calculate) surface albedo in high-latitude environments. Recent climate model intercomparison studies illustrate that models continue to struggle with albedo predictions in high latitude forests, particularly in the presence of snow (Boisier et al., 2013, 2012; Y. Li et al., 2016; Loranty et al., 2014; Qu & Hall, 2014; Wang et al., 2016). Sources of the albedo prediction error may stem from: (i) differences in the predicted snow cover extent or snowpack physical properties; (ii) differences in the albedo parameterizations themselves (i.e., the parameters that control snow canopy interception and unloading, and snow aging and melt); (iii) differences in the vegetation mapping (i.e., biogeography); and (iv) differences in structural properties of the vegetation.

Physical attributes, such as leaf area, stem area, and tree and canopy heights, are important structural controls on the surface albedo of forests (Myneni & Ross, 1991; P. J. Sellers, 1985). While recent investigations have typically focused on the prediction error arising from differences in model parameterizations of albedo (Bartlett & Verseghy, 2015; Boisier et al., 2013; Bright et al., 2015; Thackeray et al., 2014, 2015), model representations of snow physical attributes and/or spatial coverage (Boisier et al., 2013; Y. Li et al., 2016; Thackeray et al., 2015), or from differences in the vegetation mapping (Boisier et al., 2012), few studies have evaluated the prediction error attributable to differences in model representations of vegetation structure. Recent attribution analyses elsewhere have suggested that errors in simulated vegetation structure could be an important source of the persistent albedo prediction error seen in the current generation of climate models (Y. Li et al., 2016; Wang et al., 2016).

Observations suggest that variation in albedo within individual vegetation cover types is significant for forests, particularly in the presence of snow (Gao et al., 2014), most likely because of significant within-forest variation in vegetation structure. A forest classified as "evergreen needleleaf" in one region may comprise a species composition and age class structure—and hence overall structure—that is notably different to the same forest class in another region. Since resolving surface albedo (and/or other surface fluxes) for vegetated surfaces in a climate model depends on structural attributes of the vegetation, it follows that any error in the prescription or prediction of vegetation structure in time and space propagates to error in the albedo (or surface flux) prediction. Wang et al. (2016) recently found strong correlations between error in predicted forest structure (leaf area index [LAI] and tree cover fraction) and error in predicted surface albedo amongst several Coupled Model Intercomparison Project Phase 5 models during winter but did not distinguish whether the error was attributed to a poor land cover/plant functional type (PFT) specification (i.e., the vegetation mapping/biogeography) or to insufficient structural parameterizations in forests (i.e., LAI and tree cover fraction). For many of the same climate models, Li et al. (2016) found a strong correlation between LAI and wintertime albedo predictions across models but did not quantify the albedo prediction error attributable to a deficiency in the LAI prediction.

Here our primary objective is to gain additional insight into the magnitude of the albedo prediction error that is fully attributable to insufficient characterizations of forest structure. To this end, we employ a forest classification scheme (Majasalmi et al., 2018) based on national forest inventory (NFI) information that accounts for major within forest differences in structure within Fennoscandia (Norway, Sweden, and Finland)—a region with a large anthropogenic footprint in forests. Rather than explicitly quantify the albedo prediction error attributable to insufficient prescriptions of specific structural attributes such as tree cover fraction or LAI, for example, we do so implicitly through area-based representations of forest cover where only the number of forest cover types (i.e., classes) per unit area is allowed to vary, and where the structural attributes remain fixed for each forest cover type (class). In this way, the magnitude of the albedo prediction error attributable to differences in forest structure can be inferred directly from differences in the forest classification. An advantage of this approach is the ability to differentiate between the error arising from differences in the vegetation mapping from that which arises from an insufficient characterization of forest structure. A further advantage of the approach is the ability to assess the skillfulness by which climate models are able to faithfully represent gross albedo transitions in managed forests; that is, albedo changes over time per unit of forest area. Unlike other vegetation cover types, structural transitions in forests—particularly in alpine and boreal environments—play out over much longer time scales. In transient climate model simulations of prescribed land use/land cover change (LULCC), poor initial parameterizations of forest structure can result in substantial albedo prediction error, particularly when forcings or feedbacks are integrated over longer time scales. Although some climate models assimilate optical satellite information to constrain important structural parameters locally when compiling present-day surface data sets (Lawrence & Chase, 2007), this information may be lost in prognostic simulations involving managed lands, where future vegetation structure must still be prescribed over longer time horizons (W. Li et al., 2017; Pongratz et al., 2018). Further, structural information such as LAI derived from optical satellite remote sensing is biased low in boreal coniferous forests and is hence unreliable (Heiskanen et al., 2012; Serbin et al., 2013; Tian et al., 2004; Wang et al., 2016).

Since many climate models rely on land cover-dependent (or rather, PFT-dependent) lookup tables of key structural parameters for computing surface albedo (Clark et al., 2011; Oleson et al., 2013; Reick et al., 2012), the ability to faithfully represent gross structural transitions in managed forests—and the associated

albedo changes over time—is ultimately constrained by the number of forest cover (forest plant functional) types included in the model and the validity of their structural parameters. Hence, increasing the number of forest classes (or PFTs) to account for structural differences at varying successional stages represents one option for improving albedo predictions in climate modeling simulations involving transient LULCC (i.e., forest management). We hypothesize that ignoring gross structural transitions in transient forest management simulations can lead to poor albedo predictions with noteworthy climate ramifications. Thus, a second research objective is to quantify the impact of excluding gross structural transitions on the simulated surface albedo of a managed forest. This is carried out by comparing albedo predictions over an extended time span based on two classifications: one that does not distinguish between within class variations in forest structure, and one that does. Albedo differences over time between the two simulations are quantified in terms of a radiative forcing (RF) and an associated CO_2 equivalent effect.

2. Materials and Methods

2.1. Workflow Summary

Our analysis comprises three main components: (1) quantification of land cover-dependent albedos, (2) quantification of albedo prediction error and associated RF attributable to insufficient characterization of forest structure, and (3) quantification of the RF impact of not accounting for gross structural transitions when simulating transient LULCC. Land cover-dependent albedos for snow-free and snow-covered surfaces are first derived with Moderate Resolution Imaging Spectroradiometer (MODIS) Bidirectional Reflectance Distribution Function/Albedo (Lucht et al., 2000; Schaaf et al., 2002) retrievals and three alternate classifications of forest cover in Fennoscandia. The first classification is based on the latest, off-the-shelf version of the global land cover product of the European Space Agency's Climate Change Initiative (ESA CCI LC v.2.0.7 2015; Bontemps et al., 2013; European Space Agency, 2017; Hollmann et al., 2013). The second classification is based on the same ESA CCI LC product but with the forest classification modified to the 12-class scheme recently described in Majasalmi et al. (2018). The third classification is the same as the former but with an additional distinction between "Open" and "Closed" forests yielding a total of 24 forest classes. The MODIS-derived albedos are then used to predict the intrinsic surface albedos ("black-sky"/directional-hemispheric and "white-sky"/bidirectional-hemispheric) of several broadbands (near infrared, visible (VIS), entire SW) for four regional subsets under present-day land surface conditions, with predictions subsequently compared to MODIS albedo retrievals and error computed. Finally, we simulate time-dependent albedo transitions connected to a 96-year forest management scenario in which forest cover classifications are based on both the original ESA product and the modified 12-class ESA product described above, quantifying the difference in predicted albedo between the two simulations in terms of RF and CO_2 equivalent emissions.

2.2. Land Cover Classification

The Fennoscandic region (Figure 1) is a region characterized by steep topographical gradients and wet, mild climates to the west, and by increasingly flat terrain with more continental climates to the east. One pine (Scots pine, *Pinus sylvestris* L.), one spruce (Norway spruce, *Picea abies* H. (L.) Karst), and two birch species (Downy birch, *Betula pubescens* Ehrh.; Silver birch, *Betula pendula* Roth) comprise ~95% of all forest area found in the region (KSLA, 2015; Luke, 2012; Skrøppa, 2012).

The reference land cover classification for Fennoscandia is based on the latest version (v2.0.7 2015) of the global ESA CCI LC product (European Space Agency, 2017), which includes 22 main land cover classes with 15 subclasses mapped to ~300 m spatial resolution. The ESA classification in the Fennoscandic domain (mainland areas of Norway, Sweden, and Finland) includes 19 of the 22 main classes and 7 of the 15 subclasses. The main forest classes include *broadleaved deciduous*, *needleleaved deciduous*, *needleleaved evergreen*, and *mixed forest*. No distinction between "Closed" (>40% tree cover) and "Open" (15%–40% tree cover) forest subclass is made in the region. Larch (*Larix* spp.) and other deciduous needleleaved tree species occur in such limited abundance in our study domain (< 0.003% of total domain area) that they were reclassified as deciduous broadleaved forest.

Majasalmi et al. (2018) recently applied NFI data to enhance forest classification in the ESA CCI LC product (v2.0.7 2015) for the Fennoscandian region using a classification scheme that groups forest stands by both dominant tree genera and development stage using Euclidean distance-based classifiers. The enhanced

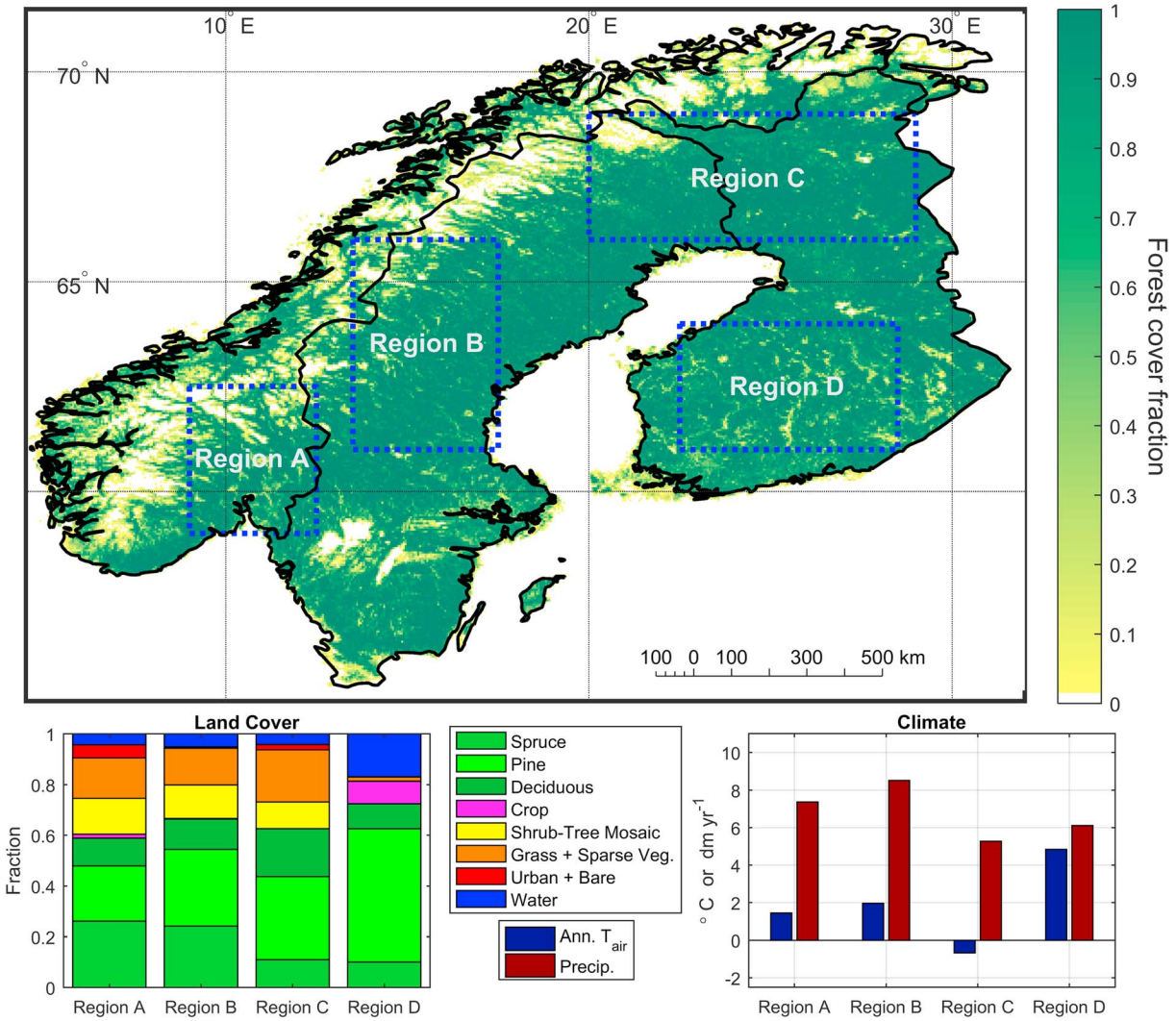

Figure 1. Overview of the spatial extent of the four regional subsets, 2015 land cover fraction in the four regional subsets, and annual mean air temperature and precipitation of the four regional subsets (2001–2011 mean; Willmott & Matsuura, 2001). Forest cover fraction is based on Majasalmi et al. (2018).

forest classification comprises a total of 12 forest classes: three main classes (based on dominant genera) and four subclasses (based on development stage). The 12 classes replace the original forest classification in the ESA product (see Majasalmi et al. (2018) for details). Illustrated in Table 1, increases in development stage (subclass) correspond to higher stem volume densities, higher maximum leaf area indices (LAIs), higher basal-area-weighted heights ("Lorey's height"), and longer crown lengths.

Because the mapping in Majasalmi et al. (2018) was based on high-resolution NFI data ($\leq$ 30 m), the subclass distinction between "Open" and "Closed" forest could be included for the study region, thus representing a second alternate classification comprising 24 forest classes (3 genera $\times$ 4 development stages $\times$ 2 tree cover fractions). The same nonforest land cover types were used for all three classifications.

2.3. Land Cover-Dependent Surface Albedo

We adopt an albedo parameterization ("Type 3" in Qu & Hall, 2007) that is widely employed in climate research (Betts, 2000; Essery, 2013; Myhre et al., 2005; Qu & Hall, 2014; Thackeray et al., 2015) where the total pixel albedo is described as a linear combination of the individual land cover albedos—themselves being a linear combination of their snow-free and snow-covered albedos weighted by the fraction of the pixel covered in snow:

Table 1
Overview of Structural Attributes Per Forest Cover Class in the Study Region (Norway, Sweden, and Finland) According to Lookup Table Values Presented in Majasalmi et al. (2018) Based on Regional NFI Data

	LAI_{MAX}	H_L	CL	VOL
ESA CCI LC, *n* forest class = 3				
Evergreen needleleaf forest (ENF)	3.9	14	9.3	147
Mixed forest (MF)	3.7	12.9	8.5	127
Deciduous broadleaf forest (DBF)	3.3	11	6.7	92
Modified ESA CCI LC, *n* forest class = 12				
Spruce 1 (S1)	1.4	7.5	6.3	22
Spruce 2 (S2)	4.3	12.3	10.1	92
Spruce 3 (S3)	6.7	16.8	13.2	201
Spruce 4 (S4)	9.1	22.0	15.8	374
Pine 1 (P1)	0.9	7.5	4.6	21
Pine 2 (P2)	2.4	11.6	6.7	80
Pine 3 (P3)	2.3	17.0	9.4	130
Pine 4 (P4)	4.4	17.2	8.4	236
Deciduous 1 (D1)	0.5	4.9	3.2	7
Deciduous 2 (D2)	1.8	8.4	5.5	36
Deciduous 3 (D3)	3.9	12.2	7.9	98
Deciduous 4 (D4)	7.0	18.3	10.3	227

Note. Values for "evergreen needleleaf forest" of the original ESA classification (top rows) are the means of all "spruce" and "pine" classes. Values for "mixed forest" of the original ESA classification are the means of all forest classes. Values for "deciduous broadleaf forest" of the original ESA classification are the means of all "deciduous" classes. "LAI_{MAX}" = Maximum growing season leaf area index (m^2/m^2); "H_L" = Lorey's (or basal-area weighted) height (m); "CL" = Crown length (m); "VOL" = stem volume density (m^3/ha^2).

$$\alpha = f_{sc}\sum_{i=1}^{n} lc_i\alpha_{i,sc} + (1 - f_{sc})\sum_{i=1}^{n} lc_i\alpha_{i,sf} \quad (1)$$

where lc_i is the pixel fraction of land cover type (or class) i, n is the total number of land cover types, f_{sc} is the pixel fraction covered in snow, and $\alpha_{i,\,sc}$ and $\alpha_{i,\,sf}$ are the albedos of land cover type i under snow-covered and snow-free conditions, respectively. In this albedo parameterization, any variation in vegetation structure within a given land cover type i is assumed to have no effect on α_{sc} and α_{sf}. Further, parameters $\alpha_{i,\,sc}$ and $\alpha_{i,\,sf}$ are insensitive to local environmental factors influencing the albedo of vegetation canopies and of snow at the surface.

We employ linear spectral "unmixing" (Bioucas-Dias et al., 2012; Keshava & Mustard, 2002; Kuusinen et al., 2013) to estimate $\alpha_{i,\,sc}$ and $\alpha_{i,\,sf}$ as regression coefficients minimizing the sum of squared residuals between predictions made with equation (1) and the empirical record. Ordinary least squares regression is performed for the original ESA CCI LC product, for the 12-class forest-enhanced ESA CCI LC product, and for the 24-class forest-enhanced ESA CCI LC product described above. Prior to the regressions, land cover classes (or subclasses) occupying less than 1% of the total domain area are merged with other similar classes to avoid poorly scaled independent variable matrices (merging is reflected in the label codes of Figure 2). Merged area comprises 3.7% of the total area within our study domain.

We rely on MODIS product MCD43C Bidirectional Reflectance Distribution Function/Albedo v005 (NASA LP DAAC, 2017) retrievals for both α and for f_{sc} at ~5,600-m spatial resolution. Albedo composites are produced every 8 days based on a 16-day window of surface reflectance observations (Schaaf et al., 2002). We include all composites dates between January 2001 and December 2011 flagged as "best quality, 75% or more with best full inversions" (i.e., integer value 0) with solar zenith angles $<70°$ (Schaaf et al., 2011) and discard everything else. The 2001–2011 means for all nondiscarded α and f_{sc} retrievals on each composite date (n = 46 $year^{-1}$) are first computed and then averaged with means of other composite dates falling within the same month (n = 3–4 $mon.^{-1}$) to obtain monthly means.

2.4. Albedo Prediction Error and RF of Albedo Prediction Error

After deriving α_{sc} and α_{sf} from the linear unmixing regression approach described above (representing the means for each land cover type i), we then apply equation (1) to calculate the albedo for each pixel (~5,600 m) falling within the four regional subsets presented in Figure 1.

The regional subsets exhibit a range of species compositions and annual climate regimes characteristic of the Fennoscandic boreal forest domain. Monthly mean albedo prediction error in forests is computed as the difference between the albedo predicted with equation (1) and that obtained from the monthly mean MODIS (MCD43C v005) record:

$$E_{p,m} = \alpha_{MODEL,p,m} - \alpha_{MODIS,p,m} \quad (2)$$

where $E_{p,\,m}$ is the prediction error in pixel p and month m, and $\alpha_{MODEL,\,p,\,m}$ and $\alpha_{MODIS,\,p,\,m}$ are the monthly mean predicted and monthly mean MODIS-retrieved albedos, respectively, in pixel p in month m. Absolute monthly mean prediction error is given as

$$\overline{E}_{p,m} = |\,\alpha_{MODEL,p,m} - \alpha_{MODIS,p,m}\,| \quad (3)$$

and the absolute error attributable to differences in the characterization of forest structure is given as

$$\widehat{E}_{p,m} = \overline{E}_{ESA,p,m} - \overline{E}_{ALT.,p,m} \quad (4)$$

where $\overline{E}_{ESA}$ is the absolute error when $\alpha_{i,\,sc}$ and $\alpha_{i,\,sf}$ in equation (1) are based on the three-class forest classification in the original ESA CCI LC product, and where $\overline{E}_{ALT}$ is the absolute error when $\alpha_{i,\,sc}$ and $\alpha_{i,\,sf}$ are based

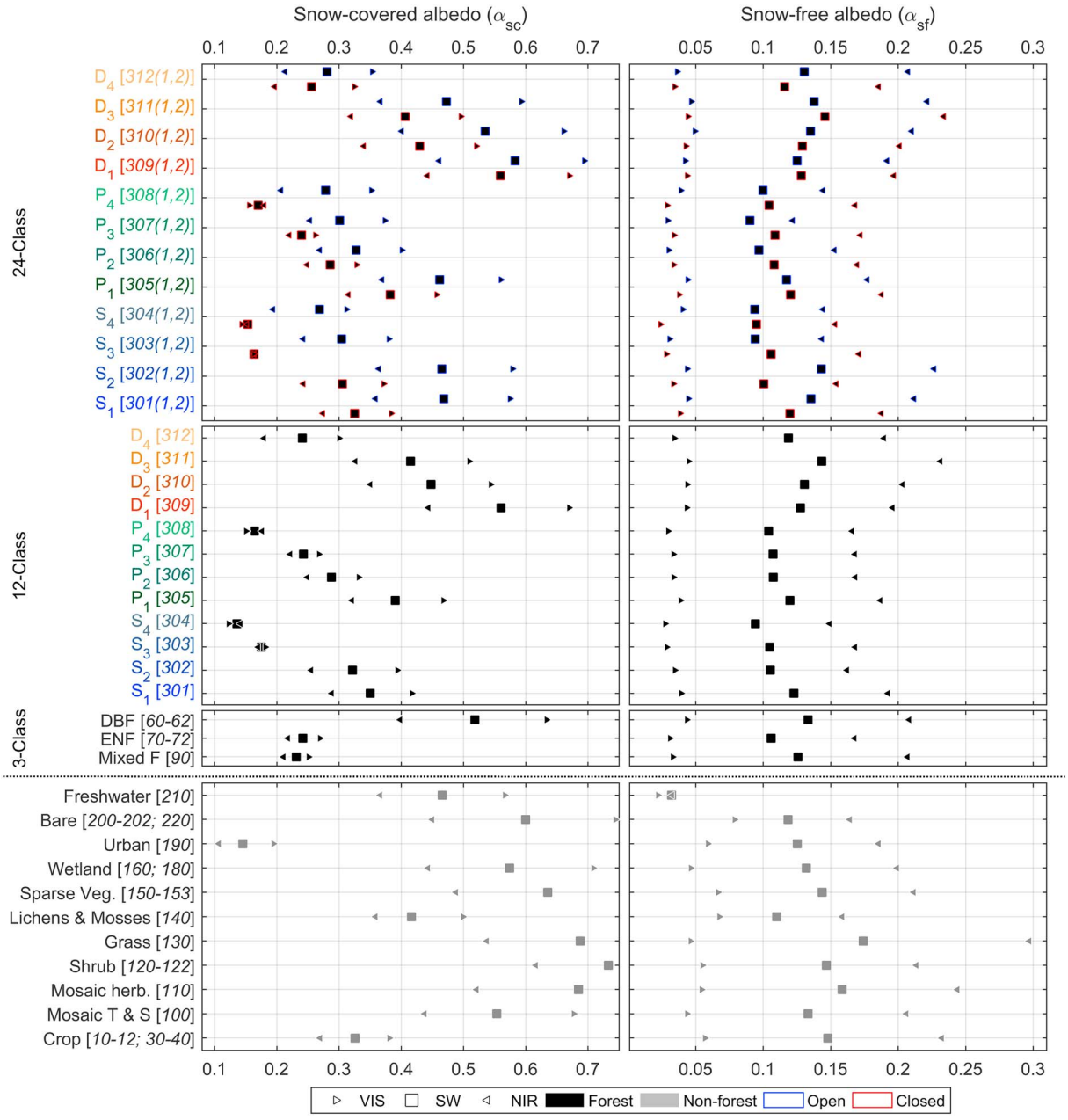

Figure 2. Land cover cover-dependent white-sky albedos as fits from ordinary least squares regressions using the model presented as equation (1). "DBF" = deciduous broadleaf forest; "ENF" = evergreen needleleaf forest; "VIS" = visible band (300–700 nm); "NIR" = near-infrared band (700–5,000 nm); "SW" = shortwave (300–5,000 nm); "Open" = >15% to <40% tree cover; "Closed" = >40% tree cover. For black-sky albedos, see Tables A1–A3 of the Appendix.

on one of the alternate classifications (i.e., the 12- or 24-class forest-modified ESA CCI LC product). Note that with equation (4), any errors related to insufficient parameterization of local environmental controls of surface albedo are effectively removed.

Monthly and annual mean albedo prediction error is expressed in terms of a monthly and annual mean RF through application of radiative kernels. Radiative kernels relate the local SW imbalance at top of the atmosphere to a change in albedo at the surface (Shell et al., 2008; Soden et al., 2008). Here the radiative kernels are derived from a 3-D, four-spectral band, eight-steam radiative transfer model (Myhre et al., 2007) based on a discrete ordinate method (Stamnes et al., 1988). The model—parameterized with 2004 atmosphere data (Dee et al., 2011) and run at 3 hr time steps—has a horizontal resolution of 1° × 1° and a vertical resolution

of 40 layers. Local RF (i.e., at MODIS pixel resolution) is therefore dependent on the mean atmospheric reflectance, transmission, and absorption properties of the coarser 1° × 1° kernel.

Monthly mean RF of the monthly mean albedo prediction error is computed as

$$RF_{E,p,m} = 100 K_{p,m} E_{p,m} \quad (5)$$

where $K_{p,\,m}$ is the radiative kernel or the change to the SW radiation flux at top of the atmosphere per 0.01 decrease in albedo at surface in pixel p and month m (in W/m^2).

2.5. Transient Forest Management Simulation

Many climate modeling studies of transient anthropogenic LULCC do not account for gross structural transitions in forests (Pongratz et al., 2018). While some effort has been undertaken to include the carbon cycle perturbation associated with forest harvests in climate models (Lawrence et al., 2012; Reick et al., 2013), the corresponding change to forest structure and the resulting perturbation to surface albedo and other climate effects are still mostly ignored. An exception here is the recent modeling study by Naudts et al. (2016) who accounted for structural transitions in the model by updating the structural parameters within each forest PFT at each time slice. Our interest here is in gaining a better understanding of the implication of *not* accounting for gross transitions in forests. Unlike the Naudts et al. (2016) approach, however, structural transitions here are implemented by updating the land cover map itself rather than the land cover (or PFT)-dependent structural parameters. To this end, a 96-year forest management scenario in Region A (Figure 1) is constructed where surface albedo is first predicted for a reference case with albedo parameters $\alpha_{i,\,sc}$ and $\alpha_{i,\,sf}$ based on the original ESA 3-class forest classification and where no structural transitions occur following disturbance events like harvests (i.e., "ENF" [evergreen needleaved forests] remains ENF)—as would be done in many modeling studies of prescribed land cover change that rely on updates to PFT area to account for structural changes on land (W. Li et al., 2017; Pongratz et al., 2018). We then compare outcomes to an alternate case in which surface albedo is predicted using the albedo parameters of the 12-class forest classification scheme, with classification updated annually using the genus- and development class-dependent residence times shown in Figure 4b. Here forest genera (i.e., the three main classes "spruce," "pine," and "deciduous") remain fixed for each grid cell, while within-genera forest classifications (i.e., the four development classes) are allowed to evolve over time from their present-day state. Rotation lengths for spruce, pine, and birch forests are 96 years, 96 years, and 60 years, respectively, after which forests are clear-felled and development class "4" is replaced by development class "1."

2.6. CO_2 Equivalence of Local RF

Local $RF_{E,\,p,\,m}$ is converted to either an annual instantaneous or a time-accumulated CO_2 emission equivalent following the methods described in Bright et al. (2016) and presented here for the reader's convenience:

$$TIEE_{E,p} = \left(12^{-1} \sum_{m=1}^{m=12} RF_{E,p,m}\right) A_e^{-1} k_{CO_2}^{-1} \quad (6)$$

where TIEE is the local time-independent CO_2 equivalent effect of an instantaneous annual RF (in kg-CO_2-eq. m^{-2}) in pixel p, $RF_{E,\,p,\,m}$ is the mean instantaneous RF of the mean albedo error in pixel p and month m, A_e is Earth's surface area (in square meters), and k_{CO_2} is the radiative efficiency of CO_2 in the atmosphere at a concentration of 389 ppmv (1.76×10^{-15} W·m^{-2}·kg^{-1}).

For a transient albedo change scenario having a time dependency at interannual scales, CO_2 equivalence is computed as

$$TDEE_{E,p} = k_{CO_2}^{-1} Y_{CO_2}^{-1} RF \quad (7)$$

where TDEE is a column vector of time-dependent emission equivalents with length defined by the number of annual time steps included in the land management scenario (in kg-CO_2-eq. m^{-2} year^{-1}), RF is a column vector of annual global mean instantaneous $RF_{E,\,p}$ ($12^{-1} \sum_{m=1}^{m=12} RF_{E,p,m}$) but for a time-dependent albedo change scenario (in W·m^{-2}·year^{-1}), and Y_{CO_2} is a lower triangular matrix with column (row) elements as the atmospheric CO_2 fraction decreasing (increasing) with time, computed with an impulse-response function (Joos et al., 2013) and a fixed CO_2 background concentration of 389 ppmv.

The time-accumulated CO_2 equivalence for any given time slice of the transient forest management simulation described in section 2.5 represents the sum of the row elements in the vector TDEE corresponding

to the time steps within that time slice (with the first row in TDEE corresponding to the present-day time step or $t = 0$).

3. Results

3.1. Land Cover-Dependent Albedos

Figure 2 presents the land cover-dependent albedos for snow-covered (α_{sc}) and snow-free (α_{sf}) surface conditions fitted with equation (1) and subsequently employed to reconstruct albedos at the scale of the MCD43C pixel (~0.05°/~5,600 m). Only results for white-sky albedo are presented henceforth, as these are more likely representative of the actual climatological (long-term average) albedos of our study domain—a region that, on average, experiences diffuse illumination conditions >50% of the time (based on the ratio of incident-to-incoming solar radiation flux between 2001 and 2011 derived from Clouds and the Earths Radiant Energy System Energy Balanced and Filled products; Kato et al., 2012; Loeb et al., 2012). White-sky α_{sc} values tend to be ~5–10% lower than the black-sky α_{sc} values, whereas the black- and white-sky α_{sf} values are more in agreement with each other (refer to Tables A1, A2, A3 of the Appendix for a comparison of these values).

Starting with nonforest land cover types (Figure 2, bottom panels, gray markers), most values fall within observed ranges reported elsewhere (Gao et al., 2005, 2014) for an alternate land cover classification based on MODIS surface reflectance and the International Geosphere Biosphere Program (IGBP) classification scheme (Friedl et al., 2002). Notable exceptions include α_{sc} for "Crop" and "Mosaic Tree and Shrub," which are found to be ~50% and ~150%, respectively, of α_{sc} for "Croplands" and "Woody Savannahs" according to IGBP classification in similar regions. For forests (black markers, upper six panels), differences in regional α_{sc} between the ESA CCI and the IGBP classification for areas classified as "evergreen needleaved forests" and "mixed forests" are negligible. We find an α_{sc} of 0.52 for "deciduous broadleaved forests" (Figure 2, third row left panel) that is ~40% higher than the α_{sc} reported elsewhere for the same classification based on IGBP. Snow-free albedos for all vegetation classes, including forests, appear within ± 10% of those reported elsewhere for similar classifications based on IGBP (Gao et al., 2005, 2014).

The effect of forest structure clearly emerges when comparing within-genus α_{sc} values for the 12-class and 24-class schemes. For the 12-class scheme, α_{sc} decreases with increasing development stage for all genera, illustrating the clear role of canopy masking of underlying snow (Figure 2, left column, middle panel). The role of canopy masking of snow is also visible for the 24-class scheme, where less tree cover ("Open," blue values) equates to less snow masking and higher overall α_{sc} for each development stage relative to those classified as "Closed" forest (red values). Within evergreen needleleaved forests, "SW" albedo under snow-covered surface conditions (α_{sc}) ranges from 0.13 to 0.39 for the 12-class scheme and 0.16 to 0.47 for the 24-class scheme (classes "P_n" and "S_n"), whereas α_{sc} for the original 3-class scheme is fixed at 0.24 (ENF, Figure 2 third row left). For deciduous broadleaved forests, α_{sc} (SW) ranges from 0.24–0.59 for the two alternate forest classifications ("D_n").

Canopy-masking effects are less apparent for α_{sf}, reflecting the larger signal contribution from underlying soils and vegetation (Figure 2, right column). Visible band albedos (300–700 nm) are highest in snow-covered surface conditions (Figure 2, "VIS," left column) and lowest in snow-free conditions (Figure 2, VIS, right column), while the opposite tends to be true for the near-infrared band (Figure 2, 700–5,000 nm).

3.2. Albedo Prediction Error, RF of Albedo Prediction Error, and Inferred Structural Prediction Error

Figure 3 illustrates that—irrespective of which forest cover classification is applied—the range in the albedo prediction error for most months is not reduced (Figures 3a–3d, whisker and box lengths). This is because the model (equation (1)) does not account for local environmental factors influencing the albedo of forested canopies and of snow. However, the two alternate classifications lead to notable error reductions in most winter months for all regions (Figures 3a–3d), suggesting improvements to the treatment of canopy masking and important controls related to forest structure.

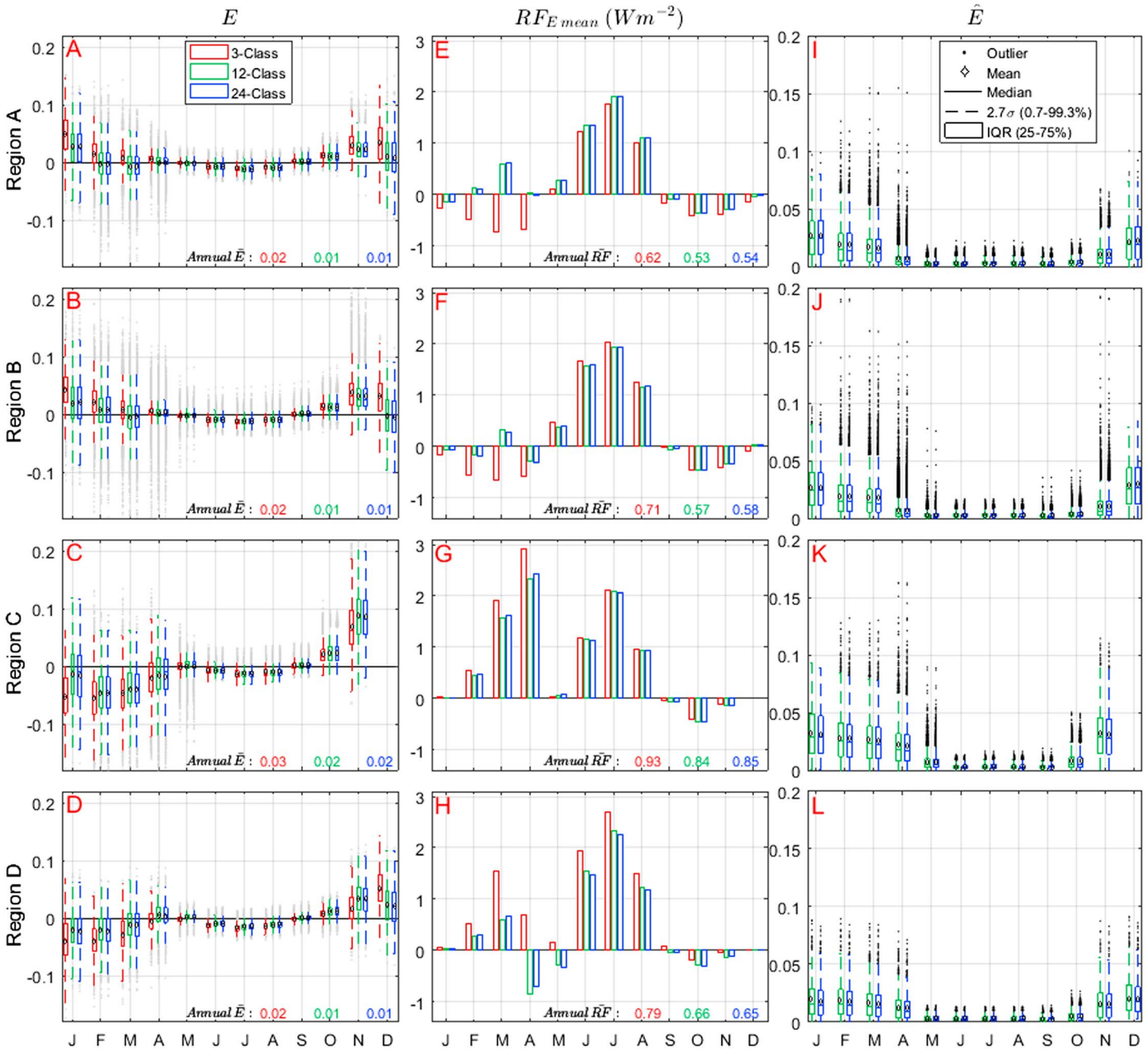

Figure 3. (a–d) Monthly surface albedo prediction error in forests (E) in each of the four regional subsets. (e–h) Monthly RF of the regional monthly mean albedo prediction error in forests, or $RF_{E\ mean} = N^{-1}\left(\sum_{p=1}^{p=N} RF_{E,p}\right)$. (i–l) Inferred surface albedo prediction error linked to forest structure, or the difference in the monthly absolute surface albedo prediction error between the 3-class and the two alternate forest classification schemes. Annual mean regional mean absolute errors are shown at the bottom for surface albedo (Figures 3a–3d) and RF (Figures 3e–3h).

Irrespective of which forest classification is applied, larger monthly mean albedo prediction error (E) is seen in Region C relative to the other three regions (Figure 3c), owing to large underprediction error in months of February–March and large overprediction error in the month of November. Relative to the other three regions, Region C is relatively cold and wet in February–March while relatively dry in November. Because the albedo parameters for snow-covered surfaces (α_{sc}) are based on average conditions, their application can underestimate the albedo of fresh snow or that of the forest canopy in colder and wetter conditions, and vice versa in warmer or drier conditions.

In this region, a lack of high-quality MODIS retrievals prevented error computation in the month of December.

For all spatial subsets, mean E is largely reduced in months of December–April when the albedo parameters of the two enhanced forest classifications are applied relative to those of the original 3-class ESA CCI forest classification (Figures 3a–3d, green and blue values versus red values). The effect of the reduced mean E seen late in the snow season (months of March and April) is more fully appreciated when measured in terms of the regional mean RF (Figures 3e–3h, right column of panels), which takes into account the increasing solar radiation loads incident at the surface. For Regions B and C, the use of the two alternative classifications reduces the RF error up to ~0.2–0.4 W/m^2 in March and April (Figures 3f and 3g). For Region A, an albedo error reduction as little as ~0.01 in April corresponds to a reduction in RF error of up to ~0.6 W/m^2 (Figure 3e, based on the mean E of the two enhanced classifications). The most notable improvements are found for Region D for the 12-class scheme, where a reduction in the March E of ~0.02 (mean) equates to a reduction in RF error of up to ~0.9 W/m^2 (Figures 3d and 3h). However, for April in this same region, the albedo and corresponding RF errors of the two alternative classifications are slightly increased in magnitude relative to predictions based on the original ESA 3-class forest classification.

In snow-free months (May–November), no systematic error reductions are detected for the two alternative forest classification schemes compared to the original 3-class product. Additionally, no systematic error reductions are seen in any season for the 24-class scheme distinguishing between "Open" and "Closed" forest types relative to the 12-class scheme, although this may not necessarily be the case for predictions in other forested regions of the study domain.

The inferred surface albedo error attributable to insufficient characterizations of forest structure is more fully visible in Figures 3i–3l, which shows differences in the absolute monthly surface albedo errors between the 3-class and the two alternate forest classification schemes or $\widehat{E}$. Such structural-related error is largest in winter (December–March), averaging ~0.02 across all subset regions and a total forest area of ~611,000 km^2. Locally, or at the scale of an individual pixel (~0.05°), $\widehat{E}$ can be as large as 0.19, which may be seen in Region B for the months of February and November (Figure 3j, outliers). These findings support the overarching research hypothesis that insufficient characterizations of forest structure can be an important source of albedo prediction error in high-latitude forests, particularly in months with snow.

3.3. Impact of Excluding Gross Structural Transitions in Forests

The impact of excluding gross structural transitions when simulating LULCC in forests is presented in Figure 4. Here this impact is expressed as the difference in the 24-year mean local predicted albedo, the associated 24-year mean local RF, and the 24-year accumulated CO_2 equivalent emission (per pixel) for four time slices in Region A.

As seen in Figure 4c, not including gross structural transitions in regional forests when simulating region forest management activities (i.e., harvest and regrowth) over the next 96 years can result in predicted surface albedo discrepancies ranging from −0.07 to 0.13 locally (24-year means). Such discrepancies are primarily related to differences in α_{sc} between the original ESA forest classes and younger (or less productive) forest classes "1" and "2" of the modified classification scheme (Figure 2). When expressed in terms of RF, such differences can range from 4 to −9 W/m^2 locally (Figure 4d, 24-year means). At present, Region A is predominately composed of older pine and spruce residing in subclasses "3" and "4" that are slated to be harvested in the next 25–50 years (Figure 4a). Hence, neglecting structural variations in regional forests over the first 24 years of the simulation leads to severe overprediction of the surface albedo (Figure 4c, first left panel)—in some areas (pixels) by as much as 0.12 (24-year mean). Taken on average for the entire region, the positive surface albedo discrepancy equates to a local RF of −1.1 W/m^2 (24-year mean). The time-accumulated TDEE for the first 24-year time slice summed over all pixels (~156,000 km^{-2}) is −4.3 Gt-CO_2-eq. As mature forests are harvested in the second 24-year time slice (Figure 4c, second panel from left), the implication of not accounting for differences in structure between young and mature forests leads to severe underprediction of surface albedo—in some areas (pixels) approaching −0.07 (24-year mean). On average, underprediction of surface albedo in the region equates to a regional annual mean RF of 0.46 W/m^2 during this period, corresponding to an accumulated CO_2-eq. emission of 1.6 Gt-CO_2-eq.

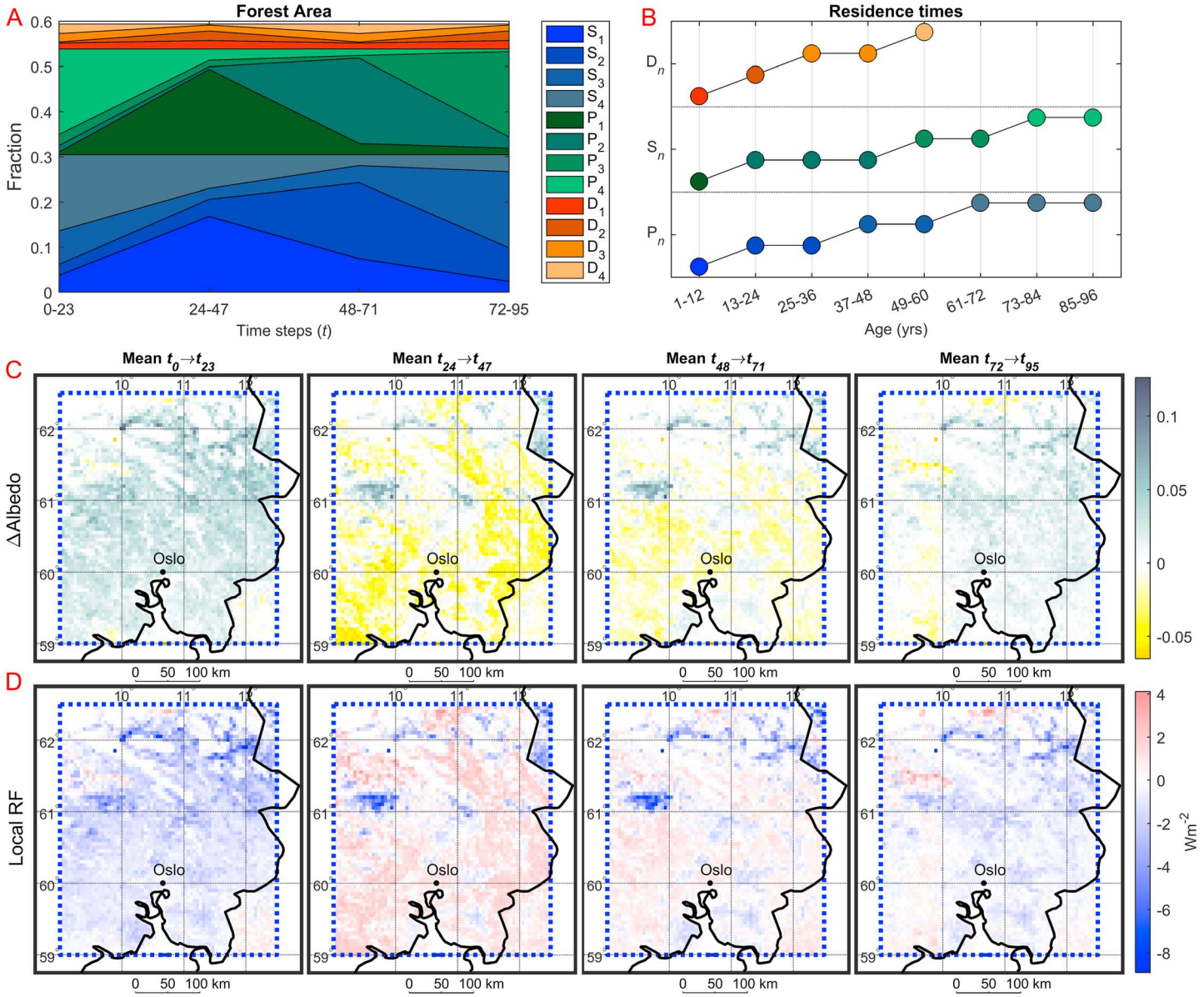

Figure 4. (a) Temporal evolution of forest area by development class and four aggregate time slices in the transient forest management simulation for Region A; (b) Residence times or the number of years that a given development class remains in that class. (c) Mean predicted local $\Delta\alpha$ ($\Delta\alpha = \alpha_{REF} - \alpha_{ALT}$) between the 3-class (reference) and 12-class (alternate) forest classification schemes for the four aggregate time slices. (d) The mean local RF of $\Delta\alpha$. Note that Figures 4a and 4b share a legend, and that "D1" replaces "D4" after 60 years. The reader is referred to Figure 3 of Majasalmi et al. (2018) for an overview of the regional distribution of the 12 forest classes.

Over the full 96-year transient simulation, the difference in predicted surface albedo between the reference (3-class) and alternative (12-class) forest classification for the region equates to an accumulated emission of -4.7 Gt-CO_2-eq. or approximately -48 Mt-CO_2-eq. year^{-1} on average.

4. Conclusions

Unraveling sources of albedo prediction error by climate models is complicated by the various ways in which surface albedo, snow characteristics and extent, and vegetation cover and structure are parameterized. The latter is further complicated by the model's reliance on key structural parameters that are vegetation (PFT) dependent, making it hard to distinguish between the error caused by erroneous mapping of the vegetation cover (i.e., biogeography) and that which is caused purely by erroneous structural characterizations. Here our

primary objective was to quantify the magnitude of the error attributable solely to erroneous structural characterizations when controlling for (i.e., eliminating) the source of the error introduced by erroneous mapping of vegetation cover. By comparing albedo predictions based on a forest classification that takes into account major structural differences at various successional stages of development (i.e., the enhanced ESA CCI LC product of Majasalmi et al., 2018) to one that does not (i.e., the original ESA CCI LC product), we were able to isolate and infer the magnitude of the albedo prediction error attributable exclusively to any difference in the representation of forest structure. Locally (i.e., at pixel scale), this structural-related error ($\widehat{E}$) was found to be as large as 0.19 in months with snow, which is on the same order of magnitude as that which may stem from poor climate model parameterizations of factors controlling canopy snow interception and unloading in boreal forests (Bartlett & Verseghy, 2015), or from deficient model parameterizations of snow metamorphosis and aging (Essery et al., 2013, 2009; Y. Li et al., 2016). When averaged across the landscape—or a total forest area of ~611,000 km^2—the mean absolute structural error from December to March was found to be as large as 0.02, equating to a mean absolute error in predicted RF of around 0.4 W/m^2 that is approximately equivalent to a pulse emission on the order of 273 Mt-CO_2-eq. (TIEE, equation (6)).

Although we have not evaluated individual climate (land) models to explicitly identify sources of error originating from insufficient characterization of any one specific structural attribute such as tree or canopy height, LAI, or tree cover fraction (among others)—our results provide a robust general indication of the improvement potential that exists by way of improved model representations of forest structure in boreal environments. Such improvement potentials are mostly confined to snow-covered conditions that can be important for improving estimates of surface albedo feedbacks (Hall, 2004; Qu & Hall, 2014; Winton, 2006). Further, results of our secondary analysis demonstrated the importance of accounting for gross structural transitions in forests when simulating surface albedo in transient land use scenarios involving forest management. We found that, for an intensively managed forestry region in Norway spanning an area as little as 156,000 km^2, the effect of ignoring gross albedo transitions in forests over the next 96 years is equivalent to not accounting for an emission of 48 Mt-CO_2-eq. year^{-1} (2016; Eurostat, 2017). Over the short term (i.e., next quarter century), given the current forest age class structure in the region, excluding gross albedo transitions is equivalent to not accounting for an emission of ~178 Mt-CO_2-eq. year^{-1} that is roughly the annual emission of a country like The Netherlands (Eurostat, 2017), or to frame it in a different perspective, about 2 days of current level global CO_2 emissions.

Improving the characterization of forest structure and accounting for gross structural transitions in climate models is crucial to instilling greater confidence in predictions that inform prospective mitigation and

Table A1
Albedo parameters for the study domain (Norway, Sweden, and Finland) Based on Regressions Using the Original ESA CCI Land Cover Product (v2.0.7 2015), 2001–2011 MODIS Albedo (MCD43C), and 2001–2011 MODIS Snow Cover Fraction (MCD43C)

	Black sky						White sky					
	SW		NIR		VIS		SW		NIR		VIS	
	α_{sf}	α_{sc}	α_{sf}	α_{sc}	α_{sf}	α_{sc}	α_{sf}	α_{sc}	α_{sf}	α_{sc}	α_{sf}	α_{sc}
Freshwater [*210*]	0.03	0.48	0.03	0.38	0.02	0.58	0.03	0.47	0.03	0.37	0.02	0.57
Bare [*200–202*; *220*]	0.11	0.60	0.16	0.45	0.08	0.74	0.12	0.60	0.16	0.45	0.08	0.74
Urban [*190*]	0.12	0.18	0.18	0.14	0.06	0.23	0.13	0.15	0.19	0.11	0.06	0.20
Wetland [*160*; *180*]	0.13	0.59	0.20	0.47	0.05	0.73	0.13	0.57	0.20	0.44	0.05	0.71
Sparse veg. [*150–153*]	0.14	0.64	0.21	0.49	0.07	0.78	0.14	0.64	0.21	0.49	0.07	0.78
Lichens and Moss [*140*]	0.12	0.43	0.16	0.38	0.07	0.51	0.11	0.42	0.16	0.36	0.07	0.50
Grass [*130*]	0.18	0.73	0.30	0.59	0.05	0.89	0.17	0.69	0.30	0.54	0.05	0.85
Shrub [*120–122*]	0.16	0.77	0.24	0.67	0.07	0.87	0.15	0.73	0.21	0.62	0.06	0.84
Mosaic herbaceous [*110*]	0.16	0.68	0.24	0.52	0.05	0.83	0.16	0.69	0.24	0.52	0.06	0.84
Mosaic tree and shrub [*100*]	0.14	0.57	0.21	0.46	0.05	0.69	0.13	0.55	0.21	0.44	0.04	0.68
MF [*90*]	0.12	0.27	0.20	0.25	0.03	0.28	0.13	0.23	0.21	0.21	0.03	0.25
ENF [*70–72*]	0.10	0.27	0.17	0.25	0.03	0.29	0.11	0.24	0.17	0.22	0.03	0.27
DBF [*60–62*]	0.13	0.53	0.21	0.41	0.04	0.65	0.13	0.52	0.21	0.40	0.04	0.63
Crop [*10–12*; *30–40*]	0.15	0.35	0.23	0.31	0.06	0.40	0.15	0.32	0.23	0.27	0.06	0.38

Note. MF = mixed forest; ENF = evergreen needleleaf forest; DBF = deciduous broadleaf forest; SW = shortwave; VIS = visible; NIR = near infrared.

Table A2
Forest Albedo Parameters for the Study Domain (Norway, Sweden, and Finland) Based on Regressions Using the Forest-Enhanced ESA CCI Land Cover Product (Majasalmi et al., 2018) With Forests Aggregated Into 12 Classes, 2001–2011 MODIS Albedo (MCD43C), and 2001–2011 MODIS Snow Cover Fraction (MCD43C)

	Black sky						White sky					
	SW		NIR		VIS		SW		NIR		VIS	
	α_{sf}	α_{sc}	α_{sf}	α_{sc}	α_{sf}	α_{sc}	α_{sf}	α_{sc}	α_{sf}	α_{sc}	α_{sf}	α_{sc}
Spruce 1 [*301*]	0.12	0.36	0.19	0.30	0.04	0.43	0.12	0.35	0.19	0.29	0.04	0.42
Spruce 2 [*302*]	0.10	0.34	0.16	0.27	0.03	0.41	0.11	0.32	0.16	0.26	0.04	0.39
Spruce 3 [*303*]	0.10	0.20	0.16	0.20	0.03	0.20	0.11	0.18	0.17	0.17	0.03	0.18
Spruce 4 [*304*]	0.09	0.18	0.15	0.20	0.03	0.16	0.09	0.14	0.15	0.14	0.03	0.12
Pine 1 [*305*]	0.12	0.42	0.19	0.35	0.04	0.49	0.12	0.39	0.19	0.32	0.04	0.47
Pine 2 [*306*]	0.11	0.31	0.17	0.28	0.03	0.36	0.11	0.29	0.17	0.25	0.03	0.33
Pine 3 [*307*]	0.10	0.27	0.16	0.25	0.03	0.29	0.11	0.24	0.17	0.22	0.03	0.27
Pine 4 [*308*]	0.10	0.20	0.16	0.22	0.03	0.18	0.10	0.16	0.17	0.18	0.03	0.15
Deciduous 1 [*309*]	0.13	0.58	0.20	0.46	0.04	0.68	0.13	0.56	0.20	0.44	0.04	0.67
Deciduous 2 [*310*]	0.13	0.46	0.20	0.36	0.04	0.55	0.13	0.45	0.20	0.35	0.04	0.54
Deciduous 3 [*311*]	0.14	0.44	0.23	0.35	0.04	0.53	0.14	0.42	0.23	0.33	0.05	0.51
Deciduous 4 [*312*]	0.12	0.27	0.19	0.21	0.04	0.33	0.12	0.24	0.19	0.18	0.03	0.30

Note. SW = shortwave; VIS = visible; NIR = near infrared.

adaptation policies involving the forestry sector. The concept of integrating forest "age cohorts" into land models is important for being able to account for time-dependent structural dynamics in secondary forests (Fisher et al., 2017; McGrath et al., 2015; Yue et al., 2018). The use of NFI data to constrain structural parameters of forest age cohorts can help ensure that the simulated structural transitions match those seen in practice. Integrating modified forest classifications into existing maps of present-day land cover (Majasalmi

Table A3
Forest Albedo Parameters for the Study Domain (Norway, Sweden, and Finland) Based on Regressions Using the Forest-Enhanced ESA CCI Land Cover Product (Majasalmi et al., 2018) With 24 Forest Classes, 2001–2011 MODIS Albedo (MCD43C), and 2001–2011 MODIS Snow Cover Fraction (MCD43C)

	Black-sky						White-sky					
	SW		NIR		VIS		SW		NIR		VIS	
	α_{sf}	α_{sc}	α_{sf}	α_{sc}	α_{sf}	α_{sc}	α_{sf}	α_{sc}	α_{sf}	α_{sc}	α_{sf}	α_{sc}
Spruce 1, closed [*3011*]	0.12	0.34	0.18	0.29	0.04	0.39	0.12	0.33	0.19	0.27	0.04	0.38
Spruce 1, open [*3012*]	0.13	0.48	0.21	0.37	0.04	0.58	0.14	0.47	0.21	0.36	0.05	0.58
Spruce 2, closed [*3021*]	0.10	0.32	0.15	0.26	0.03	0.39	0.10	0.31	0.15	0.24	0.03	0.37
Spruce 2, open [*3022*]	0.14	0.48	0.22	0.38	0.05	0.59	0.14	0.47	0.23	0.36	0.04	0.58
Spruce 3, closed [*3031*]	0.10	0.19	0.17	0.19	0.03	0.18	0.11	0.16	0.17	0.16	0.03	0.16
Spruce 3, open [*3032*]	0.09	0.30	0.14	0.24	0.03	0.37	0.09	0.30	0.14	0.24	0.03	0.38
Spruce 4, closed [*3041*]	0.09	0.20	0.15	0.20	0.02	0.18	0.10	0.16	0.15	0.15	0.02	0.14
Spruce 4, open [*3042*]	0.09	0.28	0.14	0.22	0.04	0.33	0.09	0.27	0.14	0.19	0.04	0.31
Pine 1, closed [*3051*]	0.12	0.41	0.19	0.35	0.04	0.48	0.12	0.38	0.19	0.32	0.04	0.46
Pine 1, open [*3052*]	0.12	0.49	0.18	0.40	0.05	0.58	0.12	0.46	0.18	0.37	0.04	0.56
Pine 2, closed [*3061*]	0.11	0.31	0.17	0.28	0.03	0.35	0.11	0.29	0.17	0.25	0.03	0.33
Pine 2, open [*3062*]	0.10	0.33	0.15	0.28	0.03	0.40	0.10	0.33	0.15	0.27	0.03	0.40
Pine 3, closed [*3071*]	0.11	0.27	0.17	0.25	0.03	0.28	0.11	0.24	0.17	0.22	0.03	0.26
Pine 3, open [*3072*]	0.09	0.28	0.12	0.23	0.03	0.35	0.10	0.30	0.12	0.25	0.03	0.37
Pine 4, closed [*3081*]	0.10	0.20	0.17	0.22	0.03	0.18	0.10	0.17	0.17	0.18	0.03	0.16
Pine 4, open [*3082*]	0.10	0.28	0.15	0.24	0.04	0.33	0.10	0.28	0.14	0.21	0.04	0.35
Deciduous 1, closed [*3091*]	0.13	0.57	0.20	0.46	0.04	0.68	0.13	0.56	0.20	0.44	0.04	0.67
Deciduous 1, open [*3092*]	0.13	0.60	0.20	0.48	0.05	0.71	0.13	0.58	0.19	0.46	0.04	0.69
Deciduous 2, closed [*3101*]	0.13	0.44	0.20	0.35	0.04	0.53	0.13	0.43	0.20	0.34	0.04	0.52
Deciduous 2, open [*3102*]	0.13	0.53	0.21	0.40	0.05	0.66	0.14	0.54	0.21	0.40	0.05	0.66
Deciduous 3, closed [*3111*]	0.14	0.43	0.23	0.35	0.04	0.52	0.15	0.41	0.23	0.32	0.04	0.50
Deciduous 3, open [*3112*]	0.13	0.47	0.22	0.35	0.05	0.59	0.14	0.47	0.22	0.37	0.05	0.59
Deciduous 4, closed [*3121*]	0.12	0.29	0.18	0.22	0.03	0.35	0.12	0.26	0.19	0.20	0.03	0.33
Deciduous 4, open [*3122*]	0.13	0.29	0.21	0.22	0.04	0.38	0.13	0.28	0.21	0.21	0.04	0.35

Note. SW = shortwave; VIS = visible; NIR = near infrared.

et al., 2018) can provide a spatially informed basis for constraining structural parameters of "cohort functional types" (Yue et al., 2018). However, integrating additional development classes or "cohort functional types" into models run at the global scale may impose additional computational challenges. For regional modeling studies, however, additional computational costs are minimized and such effort may be more scientifically justifiable.

Appendix A

Additional results for land cover-dependent black-sky albedos under snow-covered and snow-free conditions are presented in Appendix Tables A1–A3.

Acknowledgments
MODIS albedo and snow cover data can be obtained from the Land Processes Distributed Active Archive Center: https://lpdaac.usgs.gov/. The enhanced Fennoscandic forest classification product of Majasalmi et al. (2018) can be accessed at https://doi.org/10.21350/7zZEy5w3. The original ESA CCI land cover product can be accessed at https://www.esa-landcover-cci.org/?q=node/158. R. M. B., R. A., M. T. L, and G. M. are supported by the Research Council of Norway, grants 244074/E20 (Bio4Clim) and 254966 (QUIFFIN). T. M. is supported by the Research Council of Norway, grant 250113/F20 (TerraBGP). S. E. is supported by the Research Council of Norway, grant 243803 (I:CAN).

References

Bartlett, P. A., & Verseghy, D. L. (2015). Modified treatment of intercepted snow improves the simulated forest albedo in the Canadian land surface scheme. *Hydrological Processes*, *29*(14), 3208–3226. https://doi.org/10.1002/hyp.10431

Betts, R. A. (2000). Offset of the potential carbon sink from boreal forestation by decreases in surface albedo. *Nature*, *408*(6809), 187–190. https://doi.org/10.1038/35041545

Bioucas-Dias, J. M., Plaza, A., Dobigeon, N., Parente, M., Du, Q., Gader, P., & Chanussot, J. (2012). Hyperspectral unmixing overview: Geometrical, statistical, and sparse regression-based approaches. *IEEE Journal of Selected Topics in Applied Earth Observations and Remote Sensing*, *5*(2), 354–379. https://doi.org/10.1109/JSTARS.2012.2194696

Boisier, J. P., de Noblet-Ducoudré, N., & Ciais, P. (2013). Inferring past land use-induced changes in surface albedo from satellite observations: A useful tool to evaluate model simulations. *Biogeosciences*, *10*(3), 1501–1516. https://doi.org/10.5194/bg-10-1501-2013

Boisier, J. P., de Noblet-Ducoudré, N., Pitman, A. J., Cruz, F. T., Delire, C., van den Hurk, B. J. J. M., et al. (2012). Attributing the impacts of land-cover changes in temperate regions on surface temperature and heat fluxes to specific causes: Results from the first LUCID set of simulations. *Journal of Geophysical Research*, *117*, D12116. https://doi.org/10.1029/2011JD017106

Bontemps, S., Defourny, P., Radoux, J., Van Bogaert, E., Lamarche, C., Achard, F., et al. (2013). Consistent global land cover maps for climate modelling communities—Current achievements of the ESA's land cover CCI. Proceedings of the ESA Living Planet Symposium, Edinburgh, 9–13.

Bright, R. M., Bogren, W., Bernier, P., & Astrup, R. (2016). Carbon-equivalent metrics for albedo changes in land management contexts: Relevance of the time dimension. *Ecological Applications*, *26*(6), 1868–1880. https://doi.org/10.1890/15-1597.1

Bright, R. M., Myhre, G., Astrup, R., Antón-Fernández, C., & Strømman, A. H. (2015). Radiative forcing bias of simulated surface albedo modifications linked to forest cover changes at northern latitudes. *Biogeosciences*, *12*, 2195–2205.

Budyko, M. I. (1969). The effect of solar radiation variations on the climate of the Earth. *Tellus*, *21*(5), 611–619. https://doi.org/10.1111/j.2153-3490.1969.tb00466.x

Clark, D. B., Mercado, L. M., Sitch, S., Jones, C. D., Gedney, N., Best, M. J., et al. (2011). The Joint UK Land Environment Simulator (JULES), model description—Part 2: Carbon fluxes and vegetation dynamics. *Geoscientific Model Development*, *4*(3), 701–722. https://doi.org/10.5194/gmd-4-701-2011

Dee, D. P., Uppala, S. M., Simmons, A. J., Berrisford, P., Poli, P., Kobayashi, S., et al. (2011). The ERA-Interim reanalysis: Configuration and performance of the data assimilation system. *Quarterly Journal of the Royal Meteorological Society*, *137*(656), 553–597. https://doi.org/10.1002/qj.828

Essery, R. (2013). Large-scale simulations of snow albedo masking by forests. *Geophysical Research Letters*, *40*, 5521–5525. https://doi.org/10.1002/grl.51008

Essery, R., Morin, S., Lejeune, Y., & Ménard, C. B. (2013). A comparison of 1701 snow models using observations from an alpine site. *Advances in Water Resources*, *55*, 131–148. https://doi.org/10.1016/j.advwatres.2012.07.013

Essery, R., Rutter, N., Pomeroy, J. W., Baxter, R., Stähli, M., Gustafsson, D., et al. (2009). SnowMIP2: An evaluation of forest snow process simulations. *Bulletin of the American Meteorological Society*, *90*(8), 1120–1135.

European Space Agency (2017). Land cover CCI-product user guide version 2.0. Belgium. Retrieved from http://maps.elie.ucl.ac.be/CCI/viewer/download/ESACCI-LC-Ph2-PUGv2_2.0.pdf, Accessed Sept. 03, 2017.

Eurostat (2017). Greenhouse gas emission statistics. Accessed Nov. 17, 2017 at: http://ec.europa.eu/eurostat/statistics-explained/index.php/Greenhouse_gas_emission_statistics from European Commission.

Fisher, R. A., Koven, C. D., Anderegg, W. R. L., Christoffersen, B. O., Dietze, M. C., Farrior, C. E., et al. (2017). Vegetation demographics in Earth System Models: A review of progress and priorities. *Global Change Biology*, *24*(1), 35–54. https://doi.org/10.1111/gcb.13910

Friedl, M. A., McIver, D. K., Hodges, J. C. F., Zhang, X. Y., Muchoney, D., Strahler, A. H., et al. (2002). Global land cover mapping from MODIS: Algorithms and early results. *Remote Sensing of Environment*, *83*(1–2), 287–302. https://doi.org/10.1016/s0034-4257(02)00078-0

Gao, F., He, T., Wang, Z., Ghimire, B., Shuai, Y., Masek, J., et al. (2014). Multi-scale climatological albedo look-up maps derived from MODIS BRDF/albedo products. *Journal of Applied Remote Sensing*, *8*(1), 083532. https://doi.org/10.1117/1.JRS.8.083532

Gao, F., Schaaf, C. B., Strahler, A. H., Roesch, A., Lucht, W., & Dickinson, R. E. (2005). MODIS bidirectional reflectance distribution function and albedo climate modeling grid products and the variablility of albedo for major global vegetation types. *Journal of Geophysical Research*, *110*, D01104. https://doi.org/10.1029/2004JD005190b

Hall, A. (2004). The role of surface albedo feedback in climate. *Journal of Climate*, *17*(7), 1550–1568. https://doi.org/10.1175/1520-0442(2004)017%3C1550:trosaf%3E2.0.co;2

Heiskanen, J., Rautiainen, M., Stenberg, P., Mõttus, M., Vesanto, V.-H., Korhonen, L., & Majasalmi, T. (2012). Seasonal variation in MODIS LAI for a boreal forest area in Finland. *Remote Sensing of Environment*, *126*(supplement C), 104–115. https://doi.org/10.1016/j.rse.2012.08.001

Hollmann, R., Merchant, C. J., Saunders, R., Downy, C., Buchwitz, M., Cazenave, A., et al. (2013). The ESA climate change initiative: Satellite data records for essential climate variables. *Bulletin of the American Meteorological Society*, *94*(10), 1541–1552. https://doi.org/10.1175/bams-d-11-00254.1

Joos, F., Roth, R., Fuglestvedt, J. S., Peters, G. P., Enting, I. G., von Bloh, W., et al. (2013). Carbon dioxide and climate impulse response functions for the computation of greenhouse gas metrics: A multi-model analysis. *Atmospheric Chemistry and Physics*, *13*(5), 2793–2825. https://doi.org/10.5194/acp-13-2793-2013

Kato, S., Loeb, N. G., Rose, F. G., Doelling, D. R., Rutan, D. A., Caldwell, T. E., et al. (2012). Surface irradiances consistent with CERES-derived top-of-atmosphere shortwave and longwave irradiances. *Journal of Climate*, *26*(9), 2719–2740. https://doi.org/10.1175/JCLI-D-12-00436.1

Keshava, N., & Mustard, J. F. (2002). Spectral unmixing. *IEEE Signal Processing Magazine*, *19*(1), 44–57. https://doi.org/10.1109/79.974727

KSLA. (2015). *Forests and forestry in Sweden*. Accessed online Nov. 12, 2017. Sweden, Retrieved from Stockholm, http://www.forestindustries.se/news/publications--surveys/forests-and-forestry-in-sweden/ Accessed online Nov. 12, 2017.

Kuusinen, N., Tomppo, E., & Berninger, F. (2013). Linear unmixing of MODIS albedo composites to infer subpixel land cover type albedos. *International Journal of Applied Earth Observation and Geoinformation*, *23*, 324–333. https://doi.org/10.1016/j.jag.2012.10.005

Lawrence, P. J., & Chase, T. N. (2007). Representing a new MODIS consistent land surface in the Community Land Model (CLM 3.0). *Journal of Geophysical Research*, *112*, G01023. https://doi.org/10.1029/2006JG000168

Lawrence, P. J., Feddema, J. J., Bonan, G. B., Meehl, G. A., O'Neill, B. C., Oleson, K. W., et al. (2012). Simulating the biogeochemical and biogeophysical impacts of transient land cover change and wood harvest in the Community Climate System Model (CCSM4) from 1850 to 2100. *Journal of Climate*, *25*(9), 3071–3095. https://doi.org/10.1175/JCLI-D-11-00256.1

Li, W., Ciais, P., Peng, S., Yue, C., Wang, Y., Thurner, M., et al. (2017). Land-use and land-cover change carbon emissions between 1901 and 2012 constrained by biomass observations. *Biogeosciences Discussions*, *2017*, 1–25. https://doi.org/10.5194/bg-2017-186

Li, Y., Wang, T., Zeng, Z., Peng, S., Lian, X., & Piao, S. (2016). Evaluating biases in simulated land surface albedo from CMIP5 global climate models. *Journal of Geophysical Research: Atmospheres*, *121*, 6178–6190. https://doi.org/10.1002/2016JD024774

Loeb, N. G., Lyman, J. M., Johnson, G. C., Allan, R. P., Doelling, D. R., Wong, T., et al. (2012). Observed changes in top-of-the-atmosphere radiation and upper-ocean heating consistent within uncertainty. *Nature Geoscience*, *5*(2), 110–113. https://doi.org/10.1038/ngeo1375

Loranty, M. M., Berner, L. T., Goetz, S. J., Jin, Y., & Randerson, J. T. (2014). Vegetation controls on northern high latitude snow-albedo feedback: Observations and CMIP5 model simulations. *Global Change Biology*, *20*(2), 594–606. https://doi.org/10.1111/gcb.12391

Lucht, W., Schaaf, C., Strahler, A. H., & d'Entremont, R. (2000). Remote sensing of albedo using the BRDF in relation to land surface properties. In M. Verstraete, M. Menenti, & J. Peltoniemi (Eds.), *Observing land from space: Science, customers and technology* (Vol. 4, pp. 175–186). Netherlands: Springer.

Luke (2012). State of Finland's forests 2012: Criterion 4, biological diversity. Accessed online Nov. 11, 2017 at: http://www.metla.fi/metinfo/sustainability/c4-tree-species.htm

Majasalmi, T., Eisner, S., Astrup, R., Fridman, J., & Bright, R. M. (2018). An enhanced forest classification scheme for modeling vegetation-climate interactions based on national forest inventory data. *Biogeosciences*, *15*, 399–412. https://doi.org/10.5194/bg-2017-301

McGrath, M. J., Luyssaert, S., Meyfroidt, P., Kaplan, J. O., Bürgi, M., Chen, Y., et al. (2015). Reconstructing European forest management from 1600 to 2010. *Biogeosciences*, *12*(14), 4291–4316. https://doi.org/10.5194/bg-12-4291-2015

Myhre, G., Bellouin, N., Berglen, T. F., Berntsen, T. K., Boucher, O., Grini, A., et al. (2007). Comparison of the radiative properties and direct radiative effect of aerosols from a global aerosol model and remote sensing data over ocean. *Tellus B*, *59*(1), 115–129. https://doi.org/10.1111/j.1600-0889.2006.00238.x

Myhre, G., Kvalevåg, M. M., & Schaaf, C. B. (2005). Radiative forcing due to anthropogenic vegetation change based on MODIS surface albedo data. *Geophysical Research Letters*, *32*, L21410. https://doi.org/10.1029/2005GL024004

Myneni, R. B., & Ross, J. (1991). *Photon-vegetation interactions—Applications in optical remote sensing and plant ecology*. Berlin, Heidelberg, New York: Springer-Verlag. https://doi.org/10.1007/978-3-642-75389-3

NASA LP DAAC (2017). MODIS Terra + Aqua combined albedo/BRDF product MCD43C3 16-Day L3 global 0.05Deg CMG. Accessed May 13, 2017 at: https://lpdaac.usgs.gov/

Naudts, K., Chen, Y., McGrath, M. J., Ryder, J., Valade, A., Otto, J., & Luyssaert, S. (2016). Europe's forest management did not mitigate climate warming. *Science*, *351*(6273), 597–600. https://doi.org/10.1126/science.aad7270

Oleson, K., Lawrence, D., Bonan, G. B., Drewniak, B., Huang, M., Koven, C., et al. (2013). Technical description of version 4.5 of the Community Land Model (CLM). Retrieved from Boulder, CO, USA:

Pongratz, J., Dolman, H., Don, A., Erb, K.-H., Fuchs, R., Herold, M., et al. (2018). Models meet data: Challenges and opportunities in implementing land management in Earth system models. *Global Change Biology*, *24*(4), 1470–1487. https://doi.org/10.1111/gcb.13988

Qu, X., & Hall, A. (2007). What controls the strength of snow-albedo feedback? *Journal of Climate*, *20*(15), 3971–3981. https://doi.org/10.1175/JCLI4186.1

Qu, X., & Hall, A. (2014). On the persistent spread in snow-albedo feedback. *Climate Dynamics*, *42*(1–2), 69–81. https://doi.org/10.1007/s00382-013-1774-0

Reick, C. H., Gayler, V., Raddatz, T., & Schnur, R. (2012). JSBACH-The new land component of ECHAM. Retrieved from Hamburg, Germany:

Reick, C. H., Raddatz, T., Brovkin, V., & Gayler, V. (2013). Representation of natural and anthropogenic land cover change in MPI-ESM. *Journal of Advances in Modeling Earth Systems*, *5*(3), 459–482. https://doi.org/10.1002/jame.20022

Schaaf, C. B., Gao, F., Strahler, A. H., Lucht, W., Li, X., Tsang, T., et al. (2002). First operational BRDF, albedo nadir reflectance products from MODIS. *Remote Sensing of Environment*, *83*(1–2), 135–148. https://doi.org/10.1016/S0034-4257(02)00091-3

Schaaf, C. B., Wang, Z., & Strahler, A. H. (2011). Commentary on Wang and Zender—MODIS snow albedo bias at high solar zenith angles relative to theory and to in situ observations in Greenland. *Remote Sensing of Environment*, *115*(5), 1296–1300. https://doi.org/10.1016/j.rse.2011.01.002

Sellers, P. J. (1985). Canopy reflectance, photosynthesis, and transpiration. *International Journal of Remote Sensing*, *6*(8), 1335–1372. https://doi.org/10.1080/01431168508948283

Sellers, W. D. (1969). A global climatic model based on the energy balance of the Earth-atmosphere system. *Journal of Applied Meteorology*, *8*(3), 392–400. https://doi.org/10.1175/1520-0450(1969)008%3C0392:agcmbo%3E2.0.co;2

Serbin, S. P., Ahl, D. E., & Gower, S. T. (2013). Spatial and temporal validation of the MODIS LAI and FPAR products across a boreal forest wildfire chronosequence. *Remote Sensing of Environment*, *133*, 71–84. https://doi.org/10.1016/j.rse.2013.01.022

Shell, K. M., Kiehl, J. T., & Shields, C. A. (2008). Using the radiative kernel technique to calculate climate feedbacks in NCAR's community atmospheric model. *Journal of Climate*, *21*(10), 2269–2282. https://doi.org/10.1175/2007JCLI2044.1

Skrøppa, T. (2012). State of forest genetic resources in Norway. Retrieved from Ås, Norway:

Soden, B. J., Held, I. M., Colman, R., Shell, K. M., Kiehl, J. T., & Shields, C. A. (2008). Quantifying climate feedbacks using radiative kernels. *Journal of Climate*, *21*(14), 3504–3520. https://doi.org/10.1175/2007JCLI2110.1

Stamnes, K., Tsay, S. C., Wiscombe, W., & Jayaweera, K. (1988). Numerically stable algorithm for discrete-ordinate-method radiative transfer in multiple scattering and emitting layered media. *Applied Optics*, *27*(12), 2502–2509. https://doi.org/10.1364/AO.27.002502

Thackeray, C. W., Fletcher, C. G., & Derksen, C. (2014). The influence of canopy snow parameterizations on snow albedo feedback in boreal forest regions. *Journal of Geophysical Research: Atmospheres*, *119*, 9810–9821. https://doi.org/10.1002/2014JD021858

Thackeray, C. W., Fletcher, C. G., & Derksen, C. (2015). Quantifying the skill of CMIP5 models in simulating seasonal albedo and snow cover evolution. *Journal of Geophysical Research: Atmospheres*, *120*, 5831–5849. https://doi.org/10.1002/2015JD023325

Tian, Y., Dickinson, R. E., Zhou, L., Zeng, X., Dai, Y., Myneni, R. B., et al. (2004). Comparison of seasonal and spatial variations of leaf area index and fraction of absorbed photosynthetically active radiation from Moderate Resolution Imaging Spectroradiometer (MODIS) and Common Land Model. *Journal of Geophysical Research*, *109*, D01103. https://doi.org/10.1029/2003JD003777

Wang, L., Cole, J. N. S., Bartlett, P., Verseghy, D., Derksen, C., Brown, R., & von Salzen, K. (2016). Investigating the spread in surface albedo for snow-covered forests in CMIP5 models. *Journal of Geophysical Research: Atmospheres*, *121*, 1104–1119. https://doi.org/10.1002/2015JD023824

Willmott, C. J., & Matsuura, K. (2001). Terrestrial air temperature and precipitation: Monthly and annual time series (1950–1999). Retrieved from http://climate.geog.udel.edu/~climate/html_pages/README.ghcn_ts2.html

Winton, M. (2006). Amplified Arctic climate change: What does surface albedo feedback have to do with it? *Geophysical Research Letters*, *33*, L03701. https://doi.org/10.1029/2005GL025244

Yue, C., Ciais, P., Luyssaert, S., Li, W., McGrath, M. J., Chang, J., & Peng, S. (2018). Representing anthropogenic gross land use change, wood harvest, and forest age dynamics in a global vegetation model ORCHIDEE_MICT v8.4.2. *Geoscientific Model Development*, *11*(1), 409–428. https://doi.org/10.5194/gmd-11-409-2018